remote sensing

MDPI

Article

Bora Flow Characteristics in a Complex Valley Environment

Marija Bervida [1,*], Samo Stanič [1], Griša Močnik [1], Longlong Wang [2], Klemen Bergant [1,3] and Xiaoquan Song [4,5]

[1] Center for Atmospheric Research, University of Nova Gorica, Vipavska 11c, 5270 Ajdovščina, Slovenia; samo.stanic@ung.si (S.S.); grisa.mocnik@ung.si (G.M.); klemen.bergant@ung.si (K.B.)
[2] School of Remote Sensing and Information Engineering, Wuhan University, 129 Luoyu Road, Wuhan 430079, China; longlong.wang@whu.edu.cn
[3] Slovenian Environment Agency, Vojkova 1b, 1000 Ljubljana, Slovenia
[4] College of Marine Technology, Faculty of Information Science and Engineering, Ocean University of China, 238 Songling Road, Qingdao 266100, China; songxq@ouc.edu.cn
[5] Laboratory for Regional Oceanography and Numerical Modeling, Pilot National Laboratory for Marine Science and Technology (Qingdao), 168 Wenhai Middle Road, Qingdao 266237, China
* Correspondence: marija.bervida@ung.si

Abstract: This paper complements the existing studies of Bora flow properties in the Vipava valley with the study of Bora turbulence in a lower region of the troposphere. The turbulence characteristics of Bora flow were derived from high resolution Doppler wind lidar measurements during eight Bora wind episodes that occurred in November and December 2019. Based on the vertical profiles of wind velocity, from 80 to 180 m above the valley floor, the turbulence intensity related to all three spatial directions and the along-wind integral length scales related to three velocity components were evaluated and compared to the approximations given in international standards. The resulting turbulence characteristics of Bora flow in a deep mountain valley exhibited interesting behaviour, differing from the one expected and suggested by standards. The intensity of turbulence during Bora episodes was found to be quite strong, especially regarding the expected values for that particular category of terrain. The specific relationship between along-wind, lateral and vertical intensity was evaluated as well. The scales of turbulence in the along-wind direction were found to vary widely between different Bora episodes and were rather different from the approximations given by standards, with the most significant deviations observed for the along-wind length scale of the vertical velocity component. Finally, the periodicity of flow structures above the valley was assessed, yielding a wide range of possible periods between 1 and 10 min, thus confirming some of the previous observations from the studies of Bora in the Vipava valley.

Keywords: Doppler wind lidar; Bora wind; turbulence intensity; complex terrain; turbulence integral length scale

check for updates

Citation: Bervida, M.; Stanič , S.; Močnik, G.; Wang, L.; Bergant, K.; Song, X. Bora Flow Characteristics in a Complex Valley Environment. *Remote Sens.* **2021**, *13*, 4363. https://doi.org/10.3390/rs13214363

Academic Editor: Simone Lolli

Received: 31 August 2021
Accepted: 26 October 2021
Published: 29 October 2021

1. Introduction

Wind field measurements are fundamental for an accurate description of atmospheric dynamics, and therefore, for the understanding and prediction of weather development [1]. In the lower part of the troposphere, these measurements are important for a wide range of scientific studies and engineering applications. In the field of wind energy, they are crucial for the determination of the wind climate and for establishing the power curve of the wind turbine [2]. Measurements of wind speed and direction are further important for assessing the air pollution dispersion in the atmosphere [3] and for other studies, such as for revealing the structure and evolution of atmospheric rotors [4] or for investigating turbulent transport within a valley [5]. An accurate description of the wind field is vital as well for more realistic simulations in computational wind engineering (CWE) and related studies, such as the interactions between air flow and structures on the ground [6]. Wind characteristics are usually monitored using measurements from meteorological stations, where anemometers are used for measuring the wind speed and direction. Although they provide a high temporal resolution, these types of point measurements are location-wise sparse, especially in the vertical direction, where the measurements are typically acquired at a single height of approximately 10 m above the ground (AGL). The vertical spatial resolution can be improved by the use of radiosondes; however, in Slovenia, a single radiosonde is launched once per day in Ljubljana only, so wind measurements are sparse both in time and space.

In order to study the wind field, i.e., the spatial variation of the horizontal and vertical wind speed, the alternative technique to both anemometer and radiosonde measurements is remote sensing. Although there are various remote sensing devices and methods [7–9], the main remote sensing tool used in this study is lidar (acronym of "light detection and ranging"). Lidar may cover a wide spatial range of the atmosphere and, depending on the type of lidar and scanning strategy, with a high time resolution. The lidar used for the measurement of wind field presented in this study is Doppler wind lidar (DWL), whose measurement principle is, as its name suggests, based on using the Doppler frequency shift of light backscattered from aerosols [10]. Up until now, DWL has been widely accepted in the wind industry, where it presents an alternative to traditional mast-based wind sensors [11,12].

A region of Slovenia that is particularly interesting for wind studies is the Vipava valley (125 m above the sea level). Its surrounding complex orography provides an ideal setting for various atmospheric phenomena, such as the frequent episodes of Bora wind. Bora is a strong and gusty downslope wind with a variable frequency and duration, which generally appears in the presence of a low pressure center over the Adriatic sea or a high pressure cell over Central Europe, or as a combination of both. Bora is generally observed on the lee side of the Dinaric Alps along the Adriatic coast, whereas, in Slovenia, it is the strongest over the ridges of Trnovski gozd, Nanos and the Javorniki plateau, where it spreads into the Vipava valley. Its severe behaviour may cause damage to structures built in these regions, as well as affect traffic and pose threats to human safety in general. Mountain-induced downslope windstorms, such as Bora, are generally accompanied by multiple atmospheric phenomena, such as breaking gravity waves, hydraulic jumps, atmospheric rotors, non-stationary flow behaviour and boundary layer separation [13]. Many of these are associated with strong turbulence, which represents potential hazards to aviation. Air flow properties and atmospheric structures appearing above the Vipava valley were, up until now, studied using the ground-based measurements from Mie scattering and Raman lidar, which use aerosols as traces of air mass motion and cover the tropospheric region above a $\approx$200 m height above the valley floor. The airflow in the lower part of the atmospheric boundary layer (ABL) was regularly monitored at the bottom of the valley using anemometer point measurements at $\approx$10 m. Based on these measurements, the airflow characteristics above and within the Vipava valley were studied and various atmospheric phenomena were detected, such as hydraulic jump in the Bora flow and mountain waves above the valley [14–17]. However, there is a gap in the vertical range of the atmosphere, between 10 and 200 m above the valley floor, which, up until now, remained uninvestigated.

The main aim of this study was to complement the previous studies of atmospheric properties above the Vipava valley by obtaining insight into the flow characteristics within the uninvestigated region of the ABL above the valley. As the modeling of atmospheric flow and its phenomena, such as Bora, requires an accurate description of the wind, the study was focused on evaluating the wind profile characteristics during episodes of Bora. The mean characteristics of the Bora profile were already investigated for a Bora-affected site in Slovenia and were found to agree well with wind profile laws commonly used in computational studies [18]. However, its turbulence characteristics, needed for a more accurate description of severe Bora wind, are not fully investigated and known for Bora-affected regions in Slovenia, mostly due to the lack of proper measurement tool/setup. Therefore the aim of this study was to examine the airflow during Bora episodes in detail by evaluating the turbulence characteristics of the Bora wind profile within the complex valley region in Slovenia, which is strongly affected by Bora. For that purpose, Doppler wind lidar was used as the main tool.

2. Methodology

2.1. Measurement Site and Instrumentation

Wind measurements were acquired at the University of Nova Gorica (UNG) site in the city Ajdovščina, Slovenia (45°53′08.0″N 13°54′48.4″E). Measurement site is located in the Vipava valley (106 m above the sea level), a valley in south-west Slovenia most strongly affected by Bora. The measurement site is characterized by surrounding complex orography, as it underlies a mountain range with sharp slopes, hills and escarpments, whereas the terrain around the measurement site is characterized by regular cover of buildings (Figure 1a,b).

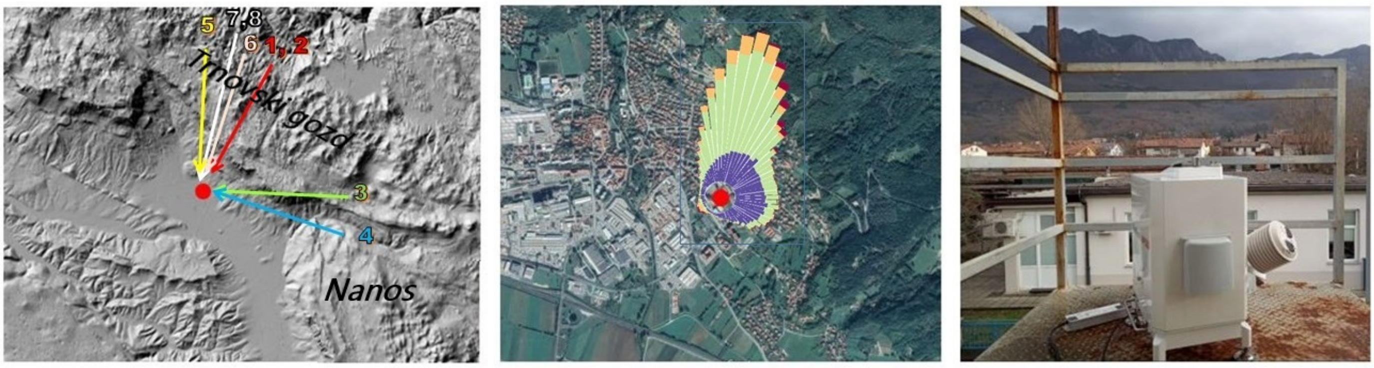

(**a**) (**b**) (**c**)

Figure 1. (**a**) The measurement site at Ajdovščina (106 m a.s.l.), marked by a red circle, is located in the Vipava valley, and surrounded by Nanos plateau (1262 m) to the north and Goli vrh (710 m) to the south. Prevailing wind directions of eight selected wind episodes are marked with different colors and numbers. (**b**) Cumulative distribution of wind direction during all selected Bora episodes at the measurement site is represented by the wind rose. (**c**) Doppler wind lidar was placed at the 10 m height AGL at the measurement site and collected measurements of radial velocity at different heights from 50–230 m AGL during November and December 2019.

Wind velocity data were collected during a one month period in November and December 2019 using a pulsed DWL WindMast WP350, manufactured by Leice Transient Technology [19], whose basic specifications are listed in Table 1. Lidar was placed at the fixed location outside the UNG building at approximately 10 m height AGL, where it recorded the radial or line-of-sight (LOS) velocity using a four beams Doppler beam swinging (DBS) scanning technique. The illustration of scanning technique is shown in Figure 2. One scanning sequence covered four lines of sights, tilted towards north (0°), east (90°), south (180°) and west (270°) direction. In each direction, measurement data were accumulated for approximately ≈ 0.916 s before it swung to the next direction. Measurements of radial velocity were collected in the vertical range of the lower troposphere from 50 to 230 m above the valley floor; more specifically, for 21 different heights: 50, 55, 60, 65, 70, 80, 90, 100, 110, 120, 130, 140, 150, 160, 170, 180, 190, 200, 210, 220 and 230 m.

2.2. Data Analysis

In order to retrieve the three-dimensional wind vector (u, v, w) from radial velocity measurements, the wind components were deduced from the four last observations assuming that flow is homogeneous across the scanning circle for each height range. Two horizontal and vertical components of wind vector were obtained from the recorded radial velocity as:

$$u_L = \frac{r_E - r_W}{2\cos\theta}, \qquad v_L = \frac{r_N - r_S}{2\cos\theta}, \qquad w_L = \frac{r_N + r_S + r_E + r_W}{4\sin\theta}, \tag{1}$$

where u_L is the horizontal east–west velocity component, v_L is the horizontal north–south velocity component, w_L is the vertical velocity component and r_N, r_E, r_S, r_W are north-tilted, east-tilted, south-tilted and west-tilted radial wind velocities, respectively. Figure 3 reports an example of time series of radial velocity measured by lidar and wind vector components, retrieved using Equation (1). The elevation angle (θ) of the laser beam was equal to 71.38° for all measurements. Wind direction α (clockwise from north) was calculated as:

$$\begin{aligned} \alpha &= \alpha_0 && \text{for} && u, v \geq 0, \\ \alpha &= 180 - \alpha_0 && \text{for} && u \geq 0, vs. \leq 0, \\ \alpha &= 180 + \alpha_0 && \text{for} && u, v \leq 0, \\ \alpha &= 360 - \alpha_0 && \text{for} && u \leq 0, vs. \geq 0, \end{aligned}$$

where $\alpha_0 = |\arctan(u_L/v_L)|$.

Table 1. Technical specifications of the Leice Doppler wind lidar WindMast WP350 [19].

Specifications	Parameter
Wavelength	1.5 µm Eye-safe
Detection height range	20–350 m
Spatial resolution	Software configurable to any 30 heights in the range 20–350 m
Range gate length	30 m (fixed)
Data updating time	1 s–10 min (configurable)
Wind speed range	0–75 m/s
Wind speed accuracy	≤ 0.1 m/s
Wind direction accuracy	< 3°

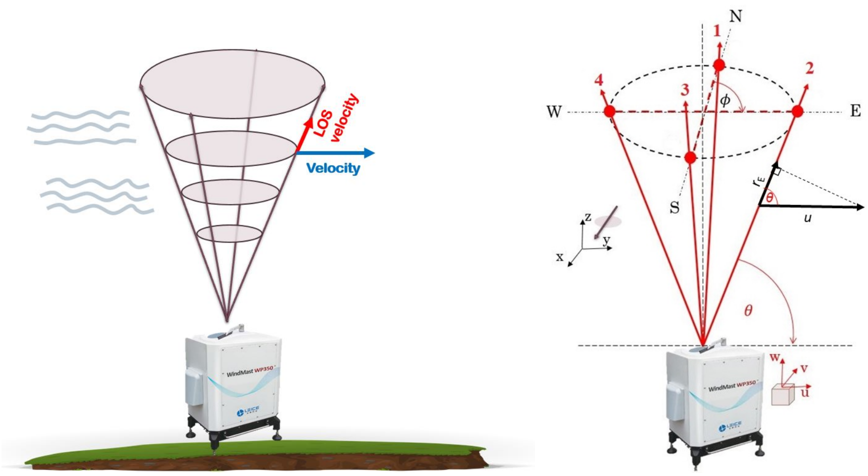

(**a**) (**b**)

Figure 2. The schematic of Doppler beam swinging scan: (**a**) visualization of scanning circles at different heights; (**b**) visualization of the four laser beams configuration of the lidar with relevant angles and two coordinate systems, one used by lidar and one used for wind analysis. For better visibility, just the component of radial velocity in the laser beam 2 direction (r_E) and component of wind vector u in the lidar coordinate system are sketched.

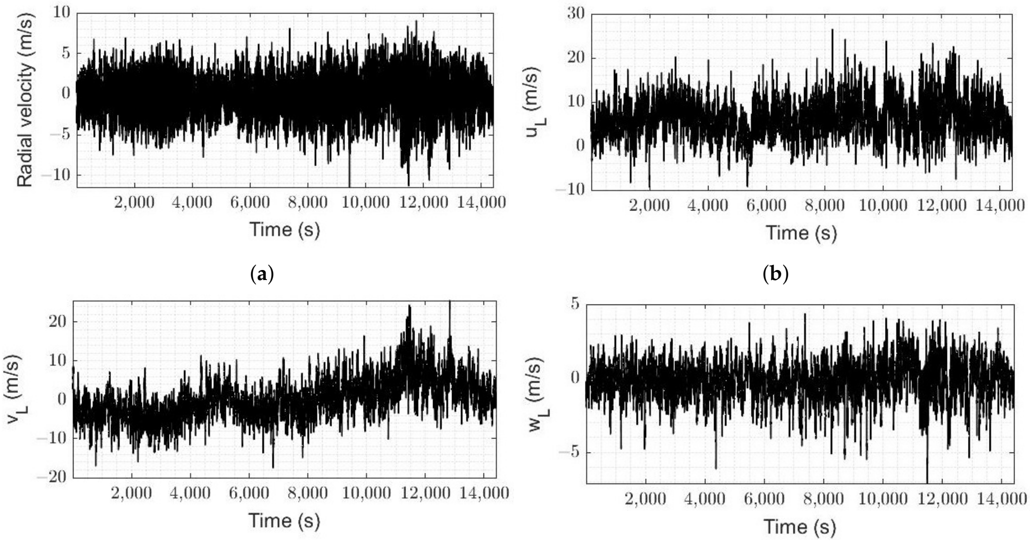

(**a**) (**b**) (**c**) (**d**)

Figure 3. An example of time series of radial velocity at 60 m AGL (**a**) and derived wind vector components: u_L (**b**), v_L (**c**) and w_L (**d**), with corresponding mean values equal to (6.40 ± 4.00) m/s, (−0.41 ± 4.86) m/s and (−0.19 ± 1.26) m/s, for a four-hour period at 3 December 2019.

Following the standard procedure for analyzing turbulence data, wind components derived in lidar coordinate system (Equation (1)) were rotated into the coordinate system aligned with mean wind direction ($\overline{\alpha}$) for each averaging period equal to 10 min. Wind vector $\mathbf{u}$ with corresponding along-wind (u), lateral (v) and vertical component (w) was calculated in our case as:

$$\mathbf{u} = \begin{bmatrix} u \\ v \\ w \end{bmatrix} = \begin{bmatrix} u_L \cos\varphi + v_L \sin\varphi \\ -u_L \sin\varphi + v_L \cos\varphi \\ w_L \end{bmatrix}$$

where φ is the angle of rotation, equal to:

$$\begin{aligned} \varphi &= 90 - \overline{\alpha} \qquad &\text{for} \qquad & 0 \leq \overline{\alpha} \leq 90, \\ \varphi &= 450 - \overline{\alpha} \qquad &\text{for} \qquad & 90 \leq \overline{\alpha} \leq 360. \end{aligned}$$

Turbulence characteristics of the air flow above the Vipava valley were assessed by means of turbulence intensity and turbulence integral length scale quantities. Turbulence intensity quantifies the intensity of wind fluctuations and was evaluated for each spatial direction. The turbulence intensity in the i-th direction (I_i) was calculated as the ratio of standard deviation of the i-th velocity component (σ_i) and the mean velocity ($\overline{U}$), for each averaging period and for each measurement height:

$$I_i = \frac{\sigma_i}{\overline{U}}. \tag{2}$$

Furthermore, by assuming the validity of Taylor's frozen turbulence hypothesis, the turbulence integral length scales in the along-wind direction were evaluated by the means of turbulence integral time scales. In particular, the turbulence integral length scale of the i-th velocity component in the along-wind (x) direction, L_i^x, was calculated by multiplying the mean velocity and the turbulence integral time scale (T_i):

$$L_i^x = T_i \cdot \overline{U}. \tag{3}$$

Turbulence integral time scales were evaluated using the autocorrelation functions R_{ii} for i-th fluctuating velocity component [20]:

$$T_i = \int_0^\infty R_{ii}(\tau)d\tau,$$

where τ is the incremental time lag. The integration of the autocorrelation function was performed to the time of the first zero-crossing of the autocorrelation function. It should be noted that, although the Taylor's hypothesis was, in general, valid for each wind episode presented here, for 6 out of 8 wind episodes, there were time intervals in which that hypothesis was not valid, as the ratio between standard deviation and mean wind speed exceeded 0.5. The length scales reported in this study serve as a rough estimate rather than exact values. Finally, in order to detect and characterize periodicity in the flow, periodograms were calculated using the Lomb–Scargle method [21].

2.3. Data Collection

There are three prevailing winds in the Vipava valley: the southeast (SE) wind, which is typically mild, the northeast (NE) wind, which corresponds to Bora and the southwest (SW) wind, which usually occur when Bora weakens [14]. Wind episodes were selected from the set of DWL data following the first main criterion, where the mean wind speed at 80 m AGL (taken as reference height) should be greater than 5.5 m/s. That value was chosen based on extrapolation of the minimal value of wind speed, which characterizes Bora at 10 m AGL [22] to a height of 80 m by the means of logarithmic wind speed law. As one of the research aims was to study the turbulence characteristics of Bora flow, 8 wind episodes were finally identified and selected for later analysis, based on prevailing wind directions and/or the synoptic situation at that time [23], which are related to Bora appearance in the Vipava valley. Their mean wind speed characteristics are summarized in Table 2 for four different heights AGL. Height profiles of the mean wind speed are reported in Figure 4 for each Bora episode analyzed in this study. Prevailing wind directions are drawn in Figure 1a, which, according to long term wind studies in the Vipava valley, agree with two main Bora wind directions, NE and SE [22]. Detailed report on wind direction is given in Figure A1 of Appendix A, where the cumulative wind speed for the heights between 80 and 180 m and direction distributions are presented in the form of wind rose for each wind episode presented in this paper.

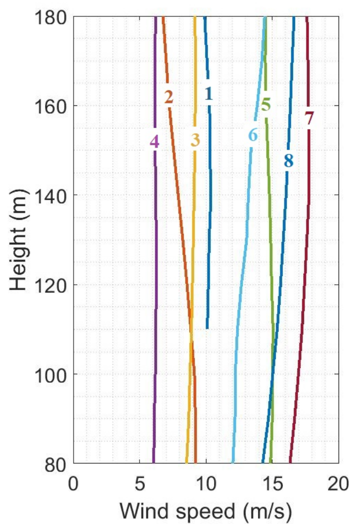

Figure 4. Height profiles of the mean wind speed for eight Bora wind episodes, marked by their ordinal numbers.

As, during November and December 2019, there were no collocated measurements of wind speed at the measurement site at the bottom height level (at 10 m AGL), the wind speed data were taken from the nearest location in the valley, provided by DARS Motorway Company [24]. These data are given just as a reference of the near-ground wind speed and do not reflect the real situation at the measurement site, as they are acquired at the location outside of the urbanization and further off of the mountain ridges, in the center of the Vipava valley. As the temperature was measured at only one height (at 10 m AGL), atmospheric stability at the site could not be retrieved. However, we consider the atmosphere to be near-neutrally stratified, as this was already shown to be the common case during Bora [18,25].

Table 2. Selected wind episodes at Ajdovščina during November 2019 and December 2019 and their characteristics. Mean wind speed and standard deviation values of selected wind episodes, calculated from 10 to min averaged DWL wind speed data at four different heights AGL, are given along with the wind speed data at 10 m AGL, calculated from 15 to min averaged wind speed data provided by DARS anemometer measurements.

Episode	Date	CET Time (hh:mm)	Duration (h)	Wind Speed at Different Heights above the Ground (m/s)				
				10 m	80 m	110 m	140 m	180 m
1	26 November 2019	10:13–12:03	1.83	2.89 ± 0.49	/	10.11 ± 5.13	10.39 ± 4.21	9.91 ± 3.82
2		12:50–15:40	2.83	2.86 ± 0.91	9.21 ± 3.05	8.86 ± 2.73	7.91 ± 2.72	6.78 ± 3.00
3	3 December 2019	8:49–12:49	4	4.80 ± 1.48	8.55 ± 3.50	8.92 ± 3.65	9.12 ± 3.87	9.19 ± 4.07
4		13:48–16:08	2.33	4.04 ± 0.84	6.07 ± 2.60	6.23 ± 2.72	6.23 ± 2.91	6.22 ± 3.08
5	4 December 2019	8:49–13:49	5	7.12 ± 2.92	14.88 ± 4.55	15.07 ± 4.34	14.80 ± 4.46	14.50 ± 5.47
6	11 December 2019	8:25–15:55	7.5	5.00 ± 1.54	12.04 ± 4.53	12.39 ± 4.50	13.21 ± 5.69	14.44 ± 7.26
7	12 December 2019	10:18–13:08	2.83	2.95 ± 0.89	16.34 ± 3.24	17.26 ± 3.00	17.78 ± 3.02	17.63 ± 3.73
8		13:45–15:05	1.33	2.64 ± 1.08	14.28 ± 2.76	15.38 ± 2.62	16.05 ± 2.45	16.66 ± 2.48

The upstream terrain orography for a 4 km horizontal distance along the prevailing wind direction is reported in Figure 5a for all selected wind episodes. It can be seen that terrain along the prevailing wind direction has the steepest slopes during wind episodes 1, 2, 6, 7 and 8, whereas there are less steep slopes for the wind episodes 3 and 5. The terrain along the prevailing wind direction of episode 4 has the lowest elevations, the smallest slant and is the least abrupt compared to other cases. In order to quantify the complexity of terrain by means of orography, the index of rugosity was used [18,26]. The magnitude of aforementioned index indicates the degree of complexity, i.e., the greater value indicates the more complex terrain. The index of rugosity with respect to prevailing wind direction of selected wind episodes is reported in Figure 5b.

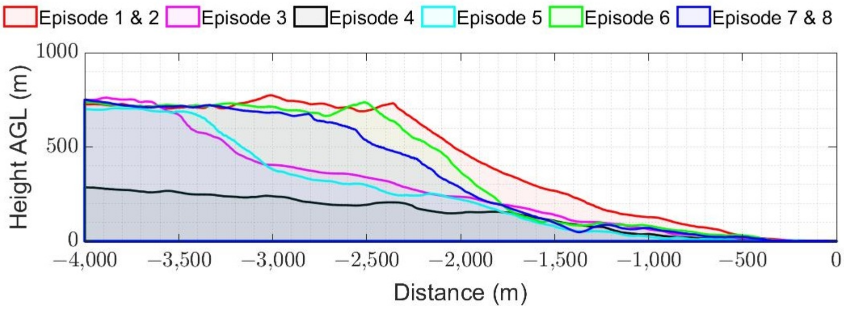

(a)

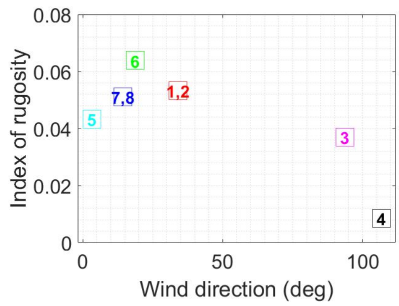

(b)

Figure 5. (**a**) Upstream terrain elevation profiles along the prevailing wind direction towards the measurement site for selected wind episodes. (**b**) The complexity of terrain with regard to prevailing wind directions of selected wind episodes, expressed by the index of rugosity [26].

2.4. Data Quality

DWL data quality can be quantified in terms of the signal-to-noise ratio (SNR), which is a measure of the relative strength of the backscattered Doppler signal over the inherent background noise. For the lidar used in this study, 6 dB is typically chosen as the lower limit for the accepted uncertainty in the measurements. Lower values of SNR are generally associated with clean air, i.e., the low concentrations of aerosols in the atmosphere [27], which is common during Bora episodes in the Vipava valley. In this study, more than 95% of measured SNR values were found to be above the lower limit (see, for example, Figure 6a). Considering the distribution of data obtained with SNR < 6 dB, reported here in Figure 6b, and considering the possible impact of data obtained with SNR < 6 dB on results and conclusions, we limit the investigation of the flow properties to 8 different heights from 110 to 180 m AGL for Bora episode 1 and to 11 different heights between 80 and 180 m for all other episodes.

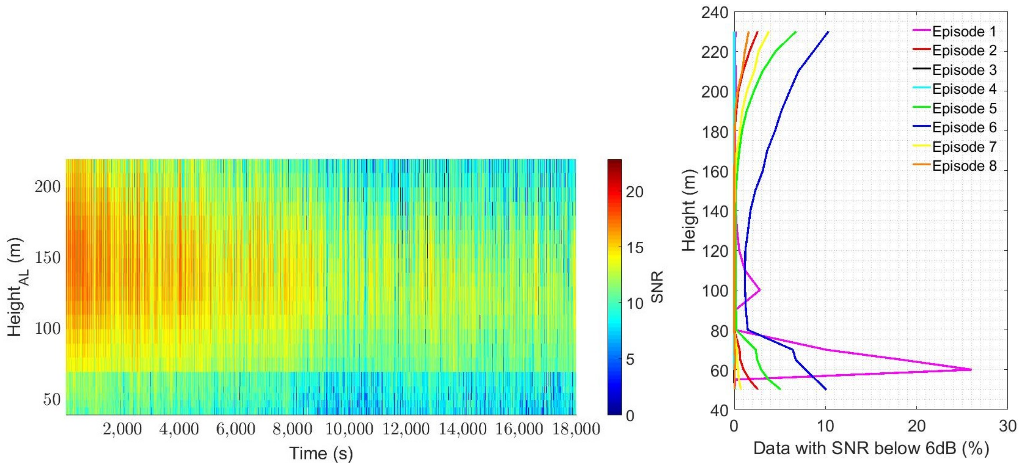

(a) (b)

Figure 6. (**a**) Time series of signal-to-noise ratio (SNR) values measured for different heights above the lidar (h_{AL}) for the measurements taken on 4 December 2019. The line at 70 m, which distinguishes two parts at the THI plot, is due to system design and does not affect the wind retrieval. (**b**) Fraction of wind speed data points with SNR values lower than 6 dB at each measurement height during a Bora episode, calculated with respect to all data points at the corresponding height.

The accuracy and calibration test for DWL used in this study was performed in 2019, just before it was deployed to Slovenia, at the flat terrain site near the village of Georgsfeld, Germany. The quality control procedure showed that the instrument does not introduce significant contribution to data inaccuracy [28]. Although the measurement site in the Vipava valley is characterized by flat-like terrain, the incoming wind is affected by the surrounding complex orography, as well as by topographical features, such as buildings, houses and trees, which may consequentially affect the accuracy of DBS measurements. Furthermore, as the flow interacting with complex topography may become horizontally non-uniform, the horizontal homogeneity assumption used for each DBS measurement sequence may be violated. Other sources that may contribute to errors in measurements are related to the flow turbulence. As the radial velocity ascribed to a certain height (center of a range gate) is, in fact, a spatially weighted average in a volume along the line of sight, the uncertainties in measured radial velocity are expected in the case of high turbulent wind fluctuations in the sampled volume [29].

3. Turbulence Characteristics of the Flow above the Vipava Valley

Turbulence characteristics of Bora flow were assessed by means of turbulence intensity in each spatial direction and the along-wind turbulence integral length scales of the flow related to fluctuations of three velocity components. Due to limitations described in Section 2.4, and based on the lidar validation tests, some degree of uncertainty is expected when evaluating these quantities. In particular, the turbulence intensity values obtained from DWL measurements during validations tests [28] were generally overestimated, but correlated fairly well to the turbulence intensity obtained from the reference (anemometer) measurements, with a squared correlation coefficient between 0.64 and 0.72 for heights above 61 m AGL [28]. The expanded uncertainty ($\pm\, 2\sigma$) was found to range from 9 to 16%

for these heights, whereas, below 61 m AGL, it was greater than 25%. As there were no reference measurements at these heights near the measurement site in the Vipava valley, we could not evaluate the exact uncertainty in our case, but we expect a similar or larger degree of uncertainty as in the validations test. Furthermore, due to the calculation procedure described in Section 2.2 and due to large uncertainties related to the DBS scanning method when measuring the turbulence in complex terrain [30], the integral turbulence length scales reported in this study should be taken as a rough approximate.

3.1. Turbulence Intensity

Turbulence intensity components in the along-wind (I_u), lateral (I_v) and vertical (I_w) direction were calculated for different heights between 80 and 180 m (Section 2.4), according to Equation (2), for 10-min time periods of selected wind episodes. In the case of flat, homogeneous terrain, the turbulence intensity is expected to decrease with height. A general expression, given by Eurocode (EC) [31], that approximates the vertical profile of (along-wind) turbulence intensity and is often used in CWE models, is given by:

$$I_u^{(EC)} = \frac{1}{\ln(h/z_0)}, \tag{4}$$

where z_0 is the aerodynamic roughness length (or surface roughness) and h is the height above the ground. If we assume that the value of z_0 varies between 0.3 m and 0.7 m for the Vipava valley terrain (according to [31,32]), then the along-wind turbulence intensity values would range up to $\approx$ 20% for the heights from 80–180 m AGL according to Equation (4). However, in this study, we have a complex valley environment, as well as a gusty wind, so the deviations from the profile described by Equation (4) are expected and were observed in the analyzed wind episodes. At first glance, we observed large values of turbulence intensity above the Vipava valley during the majority of selected wind episodes. This observation is presented in Figure 7, which reports the time evolution of the turbulence intensity components at all measurement heights, wind episode 5 being taken as the representative example.

During that particular episode (Figure 7), the turbulence intensity was mainly below 45% at the heights between 80 and 180 m, for both the along-wind and lateral component. The vertical component of the turbulence intensity reached up to a maximum of 17%, with a mean of around 10%. The mean values of the turbulence intensity at 80 m AGL, calculated from all time periods of each selected wind episode, were found to range between 20% and 51% (Figure 8a) for the along-wind component and between 20% and 50% (Figure 8b) for the lateral component, which are both larger than those predicted by the international standard (Equation (4)). The values of the vertical intensity component ranged between 6% and 16% (Figure 8c). A detailed report on turbulence intensity values and their characteristics is given in Table A1 of Appendix B for all eight analyzed episodes and for four different heights AGL. Their mean and standard deviation values are reported in Figure 8.

The turbulence intensity changed during the time of each wind episode, with a similar degree of variations at all heights (between 80 and 180 m) in general. The details are given in Table A1 of Appendix B, where the variability of turbulence intensity components is given in terms of the standard deviation. A representative example of the turbulence intensity time evolution at four different heights is given in Figure 9a for wind episode 5. Furthermore, we assessed the vertical profiles of turbulence intensity. Figure 9b reports the turbulence intensity profile in each spatial direction, represented by the mean and the envelope containing all intensity profiles obtained during wind episode 5. For the sake of conciseness, the results of other wind episodes were not plotted here, though the behavior of intensity profiles during all wind episodes was found to be similar; that is, the turbulence intensity is nearly constant or slightly decreases with the height until a certain level (in the case shown in Figure 9b, at $\approx$140 m). Interestingly, after reaching a certain height, the turbulence intensity in most of the analyzed wind episodes starts to increase with the height, which is opposed to our expectations and the relationship described by Equation (4).

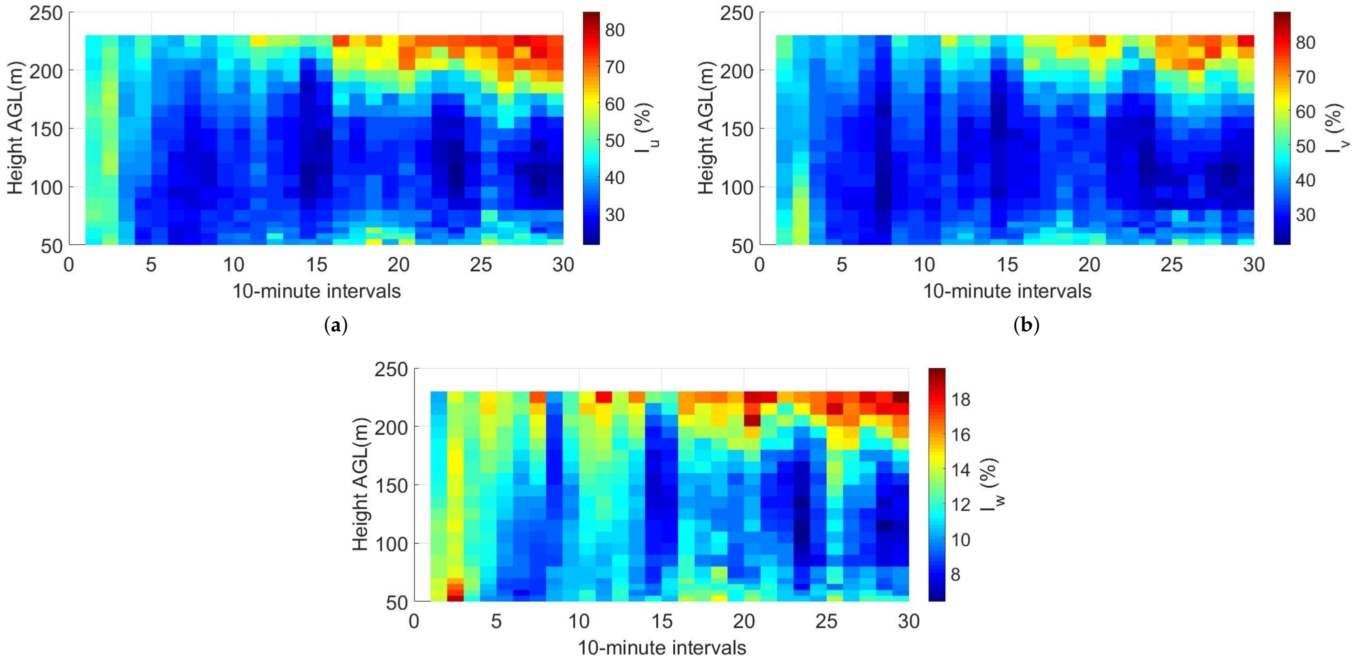

(**a**) (**b**) (**c**)

Figure 7. Time evolution of turbulence intensity for 21 different heights AGL, in the along-wind (**a**), lateral (**b**) and vertical (**c**) direction during wind episode 5 on 4 December 2019.

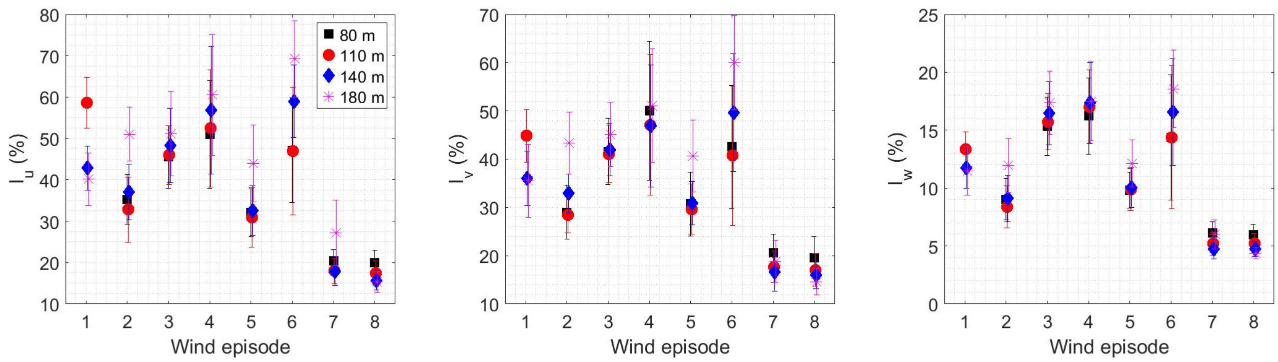

(**a**) (**b**) (**c**)

Figure 8. Mean turbulence intensity values in the along-wind (**a**), lateral (**b**) and vertical direction (**c**), obtained from Doppler wind lidar measurements at four different heights above the ground, for all eight wind episodes.

Although the turbulence intensity was expected to decrease with respect to the distance from the ground, there may be atmospheric processes in the higher levels of the ABL related to the disturbances of the airflow when passing over high mountain barriers, which surround the valley. Besides that, lower SNR values may contribute to poorer data quality at those heights (Figure 6b), which then reflects in higher values of turbulence.

From Figure 9a, as well as from previous figures (Figures 7 and 8), it may be observed that the values of turbulence intensity in the along-wind and lateral direction are comparable and considerably larger than those in the vertical direction. Ratios of lateral and vertical intensity to the along-wind component are reported in Figure 10 for wind episode 5. Figure 10a reports their time evolution at four different heights, whereas Figure 10b reports the mean vertical profiles of the aforementioned ratios, along with standard deviation.

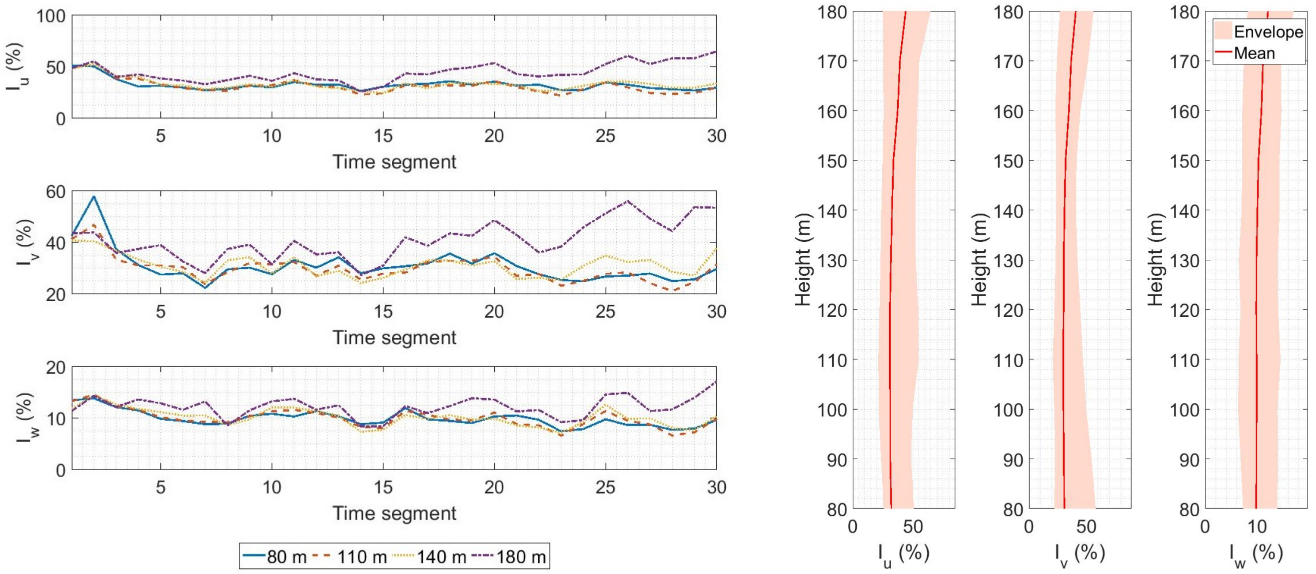

(**a**) (**b**)

Figure 9. Wind episode 5 on 4 December 2019: (**a**) time evolution of turbulence intensity components at four different heights above the ground. Each time segment represents 10 min interval; (**b**) vertical profiles of turbulence intensity components during all time intervals, represented by their envelope and mean.

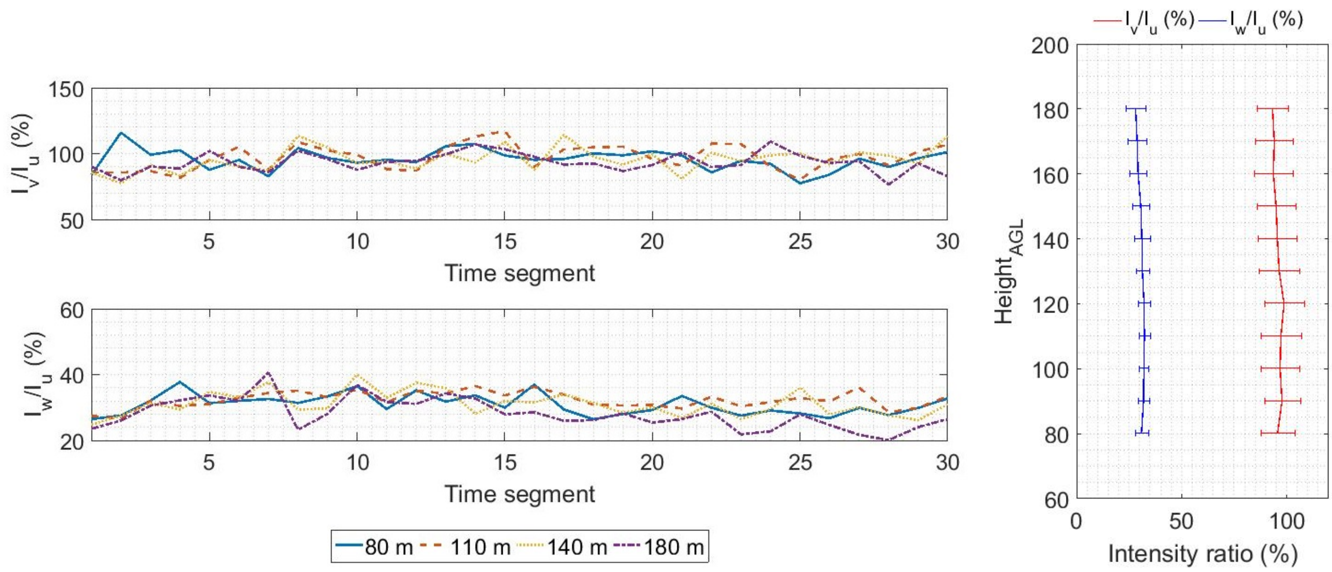

(**a**) (**b**)

Figure 10. Wind episode 5 on 4 December 2019: (**a**) time evolution of lateral (*top*) and vertical (*bottom*) turbulence intensity as a percentage of the along-wind intensity component at four different heights above the ground. Each time segment represents a 10 min interval; (**b**) mean vertical profile of the ratio between turbulence intensity components.

For all wind episodes, the ratio between turbulence intensities was found to be nearly constant with the height (Figure 9b), as it is often considered for ABL flows [33], with a slight decrease observed above a certain height (≈140 m). By considering the intensity ratios to be constant with the height, we evaluated the mean intensity ratios for each Bora episode separately and reported them in Figure 11, along with the mean of all wind episodes, as well as in Table 3 in more detail.

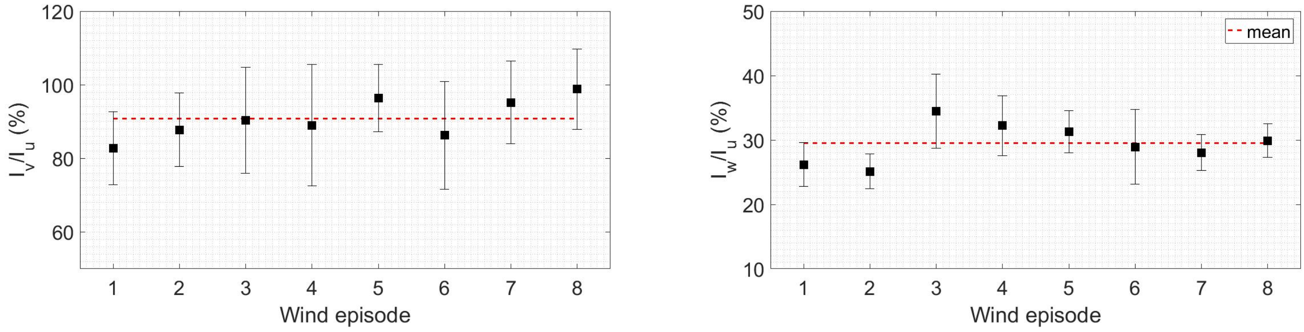

(**a**) (**b**)

Figure 11. Grand mean values of (**a**) lateral and along-wind turbulence intensity ratio and (**b**) vertical and along-wind turbulence intensity ratio, expressed as a percentage and obtained for each wind episode from the mean values of intensity ratios at 11 measurement heights, from 80 to 180 m. Red dotted line denotes the mean of all wind episodes.

Table 3. Grand mean values of lateral/vertical and along-wind turbulence intensity ratio, obtained for each wind episode from the mean values of intensity ratios at 11 measurement heights, from 80 to 180 m. The ratios are expressed as a percentage and are presented by their median, mean, standard deviation, minimum and maximum value.

Wind Episode		Median	Mean	σ	Min	Max		Median	Mean	σ	Min	Max
1		82.23	82.73	9.94	54.55	109.03		26.16	26.17	3.39	19.13	36.77
2		87.44	87.78	10.04	62.34	130.39		24.77	25.11	2.72	19.01	31.98
3		88.19	90.31	14.39	62.58	130.30		34.24	34.48	5.73	22.40	50.22
4	I_v/I_u (%)	89.78	88.99	16.52	56.23	143.15	I_w/I_u (%)	33.18	32.22	4.65	19.37	40.78
5		96.22	96.35	9.10	74.85	119.16		31.21	31.29	3.29	22.50	40.01
6		84.49	86.24	14.58	50.41	146.73		28.03	28.92	5.81	18.37	48.96
7		95.72	95.20	11.20	63.83	123.08		28.28	28.02	2.79	19.88	35.06
8		97.19	98.79	10.92	80.75	136.39		29.65	29.89	2.60	23.61	34.62

The cumulative ratio of all wind episodes analyzed in this study may be expressed as:

$$I_u : I_v : I_w = 1 : 0.9 : 0.3, \tag{5}$$

which is quite different to those suggested for ABL in [34]:

$$I_u : I_v : I_w = 1 : 0.75 : 0.5 \tag{6}$$

and [35]:

$$I_u : I_v : I_w = 1 : 0.88 : 0.55. \tag{7}$$

In the case of Bora above the complex terrain of Vipava valley, the along-wind and lateral turbulence intensity were found to be comparable and larger than approximations for the ABL given by Equations (6) and (7), whereas the intensity in the vertical turbulence intensity was found to be much smaller. Furthermore, we compared our results to results obtained for Bora flow, but at another location (Croatia) [36]. In that case, we obtained a smaller ratio between the lateral and along-wind turbulence intensity, which was, in their case, equal to 1 at 40 m AGL. The ratio between the vertical and along-wind turbulence intensity was smaller for our case, compared to their value of 0.5 at 40 m AGL. Finally, we investigated if the values of turbulence intensity at heights of above 50 m were related to underlying terrain complexity, where the terrain complexity was quantified in terms of orography, as described in Section 2.4. No correlation was found between the orographic terrain complexity and the intensity of turbulence during analyzed Bora episodes (Figure 12).

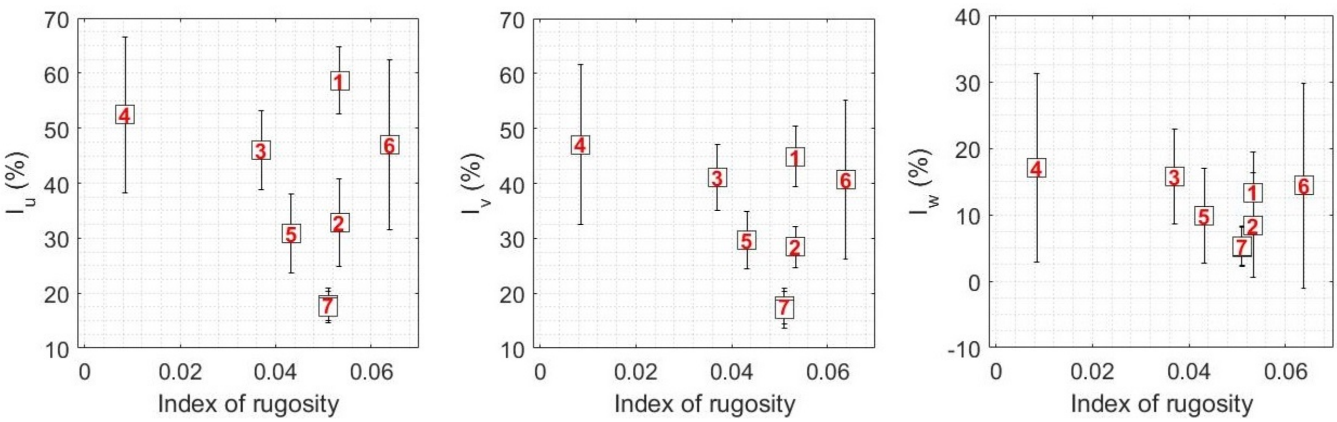

(**a**) (**b**) (**c**)

Figure 12. Turbulence intensity at 110 m AGL in the along-wind (**a**), lateral (**b**) and vertical (**c**) direction with regard to index of rugosity for different Bora episodes, labeled by their ordinal number. The index of rugosity represents the orographic complexity of the 4 km path upstream of the measurement site. Note: data points of wind episodes 7 and 8 overlap.

3.2. *Assessment of Turbulence Integral Length Scale*

The turbulent length scales of three velocity components in the along-wind direction, L_u^x, L_v^x and L_w^x, were calculated according to Equation (3), where the corresponding integrals of correlation functions were approximated using the trapezoidal rule. The mean values of along-wind turbulent length scales at four different heights are reported in Figure 13 for all wind episodes, while more details are given in Table A2 of Appendix B. At first, it can be noticed from Figure 13 that the values of along-wind length scales related to along-wind (L_u^x) and lateral velocity fluctuations (L_v^x) are comparable, whereas the values of the length-scale of vertical velocity (L_w^x) are significantly larger. Considering all Bora episodes in this study, we found that the length-scale of vertical velocity increases with height faster and reaches higher values (up to 180 m) than the other two along-wind length scales. For better readability, that observation is represented in Figure 14, where the mean values of along-wind length scales are reported for two central heights, 110 m and 140 m.

The time evolution of along-wind length scales at four different heights is reported in Figure 15a for wind episode 5, which is used as a representative of all episodes. It reveals the rough changes in the length scale values during time. The dispersion of the obtained data is reflected in high standard deviation values. Standard deviation, along with other turbulence length scales characteristic values (median, mean, standard deviation, minimum and maximum) obtained at four different heights, is given in Table A2 of Appendix B for each Bora episode.

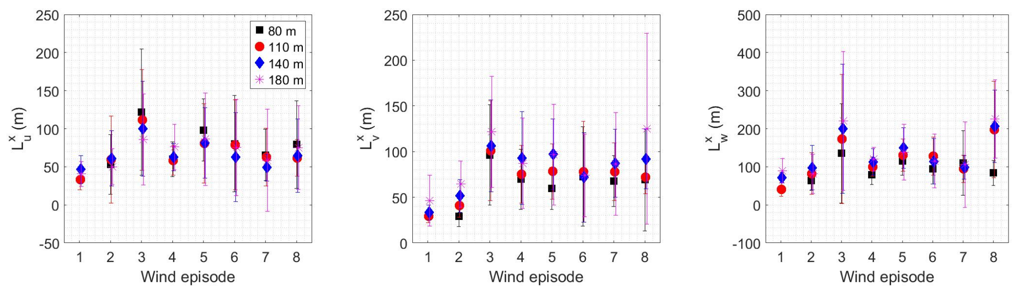

(**a**) (**b**) (**c**)

Figure 13. Mean values of along-wind turbulence length scales, obtained from Doppler wind lidar measurements at four different heights above the ground, for all eight wind episodes (**a**–**c**).

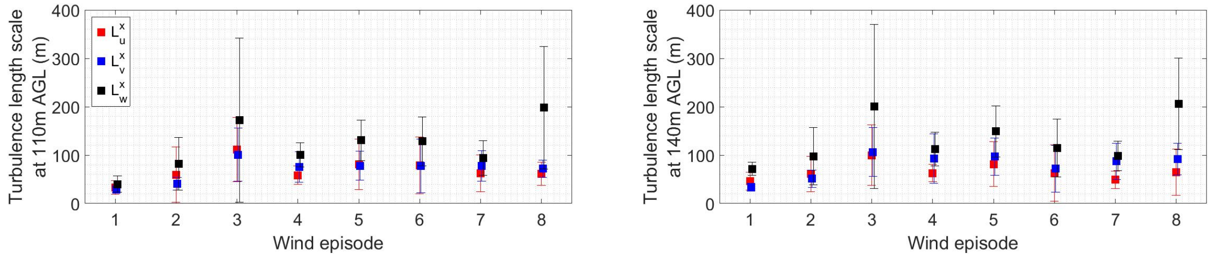

(**a**) (**b**)

Figure 14. Mean values of along-wind turbulence length scales, obtained from Doppler wind lidar measurements at 110 m AGL (**a**) and 140 m AGL (**b**) for all eight wind episodes.

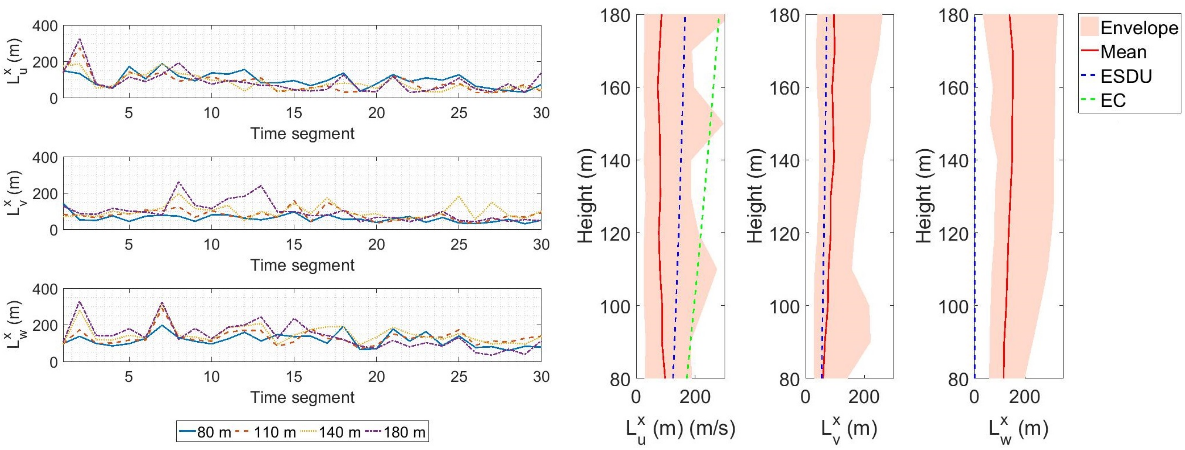

(**a**) (**b**)

Figure 15. Wind episode 5 on 3 December 2019: (**a**) time series of along-wind turbulence integral length scales at four different heights above the ground, obtained from Doppler wind lidar measurements; (**b**) vertical profiles of turbulence integral length scales, represented by their envelope and mean, along with Eurocode (EC) and ESDU approximations denoted by dashed curves.

We further investigated the vertical profiles of the along-wind length scales based on the obtained wind data at 11 different heights. Usually, turbulence integral length scales in ABL and their vertical profiles may be approximated by empirical formulas, such as those found in wind engineering standards Eurocode (EC) [31] and ESDU [37]:

$$L_u^x = 300 \cdot (h/200.0)^{0.67+0.05\cdot\ln(z_0)}, \tag{8}$$

$$L_u^x = 25 \cdot h^{0.35} \cdot z_0^{-0.063} \qquad L_v^x = L_u^x \cdot \frac{1}{2}\left(\frac{\sigma_v}{\sigma_u}\right)^3 \qquad L_w^x = L_u^x \cdot \frac{1}{2}\left(\frac{\sigma_w}{\sigma_u}\right)^3, \tag{9}$$

where h is the height above the ground, $\sigma_u, \sigma_v, \sigma_w$ are mean standard deviations of the along-wind, lateral and vertical velocity component, respectively and z_0 is the aerodynamic roughness length. However, there are still quite large uncertainties and difficulties met in providing an accurate evaluation of such quantities based only on the terrain category [38,39]. Figure 15b reports the mean along-wind turbulence length scale profiles and the envelope containing all of their values obtained during wind episode 3, along with the approximations given by Equations (8) and (9). Equations (8) and (9) were calculated by taking the roughness length value equal to 0.3 m and standard deviations obtained from DWL measurements. For the sake of conciseness, length-scale profiles of other wind episodes were not plotted here. The observations following on from all analyzed wind episodes are as follows:

1. Mean values of L_u^x, L_v^x and L_w^x did not monotonically increase with the height for all investigated Bora episodes, as suggested by standards (Equations (8) and (9)), but varied. In most wind episodes, those values both increased and decreased with the height;
2. Mean L_u^x profile was found to have smaller values than both approximations given by ESDU and EC;
3. Mean L_v^x profile was found to have larger values than approximated by ESDU;
4. While both L_u^x and L_v^x were found to moderately agree with ESDU, L_v^x showed a slightly better agreement;
5. Mean L_w^x profile was found to have considerably larger values than those approximated by ESDU, as well as having larger values than both mean L_u^x and L_v^x.

The turbulence length scales presented in this section have large uncertainties, and the values should be regarded as rough approximations. This is due to the wind measurement technique itself (DBS is not the best choice for this purpose) and also due to large differences between the results of the different length scale calculation methods (autocorrelation function integral method and auto-power spectral method were used). The autocorrelation function integral method (Equation (3)) was found to describe our data better than the auto-power spectral method.

3.3. Periodicity of the Flow above the Vipava Valley

The origin and periodic behavior of Bora flow have been an active research topic throughout decades [40–42]. In the Vipava valley, the studies of Bora and related structures appearing in the atmosphere were based on the wind speed measurements at 10 m AGL and lidar measurements, which covered the vertical extent of the atmosphere above 200 m above the valley floor. Thus, a vertical region of the atmosphere above the valley between 10 and 200 m remained uninvestigated. In previous studies, a wide range of possible wind gust periods between 1 and 7 min was identified. For ABL structures, typical oscillation periods were found to be between 1 and 2 min, whereas, for the structures above the ABL, they were found to be between 3 and 6 min [22].

In this study, we assessed the periodicity of the flow by calculating the Lomb–Scargle periodograms of the vertical wind velocity component, obtained by DWL at the 110 m height AGL, thus representing the higher vertical range of atmosphere, which was not assessed up until now. Periodograms of the vertical wind speed are reported in Figure 16 for each Bora episode, along with the dominant period between 1 and 10 min. First, we observed that a number of periods appear in the periodogram of the vertical wind speed for all Bora episodes. Based on their power, we identified the three most significant ones for each wind episode (Figure 16). A periodicity of ≈3.5 min was detected during Bora episodes 3, 4 and 5. These episodes occurred during two consecutive days, which were characterized by two different prevailing Bora directions in the valley and thus by different orography. A slightly larger period of ≈4.5 min was detected both in Bora episode 2 and 6, while it also occurred during wind episode 1. Shorter dominant periods of up to 2 min were detected during wind episodes 7 and 8 (which occurred on the same day) and during wind episode 1. Finally, multiple periods with comparable power were detected during wind episode 6, of which, the dominant period of 9 min had the greatest power.

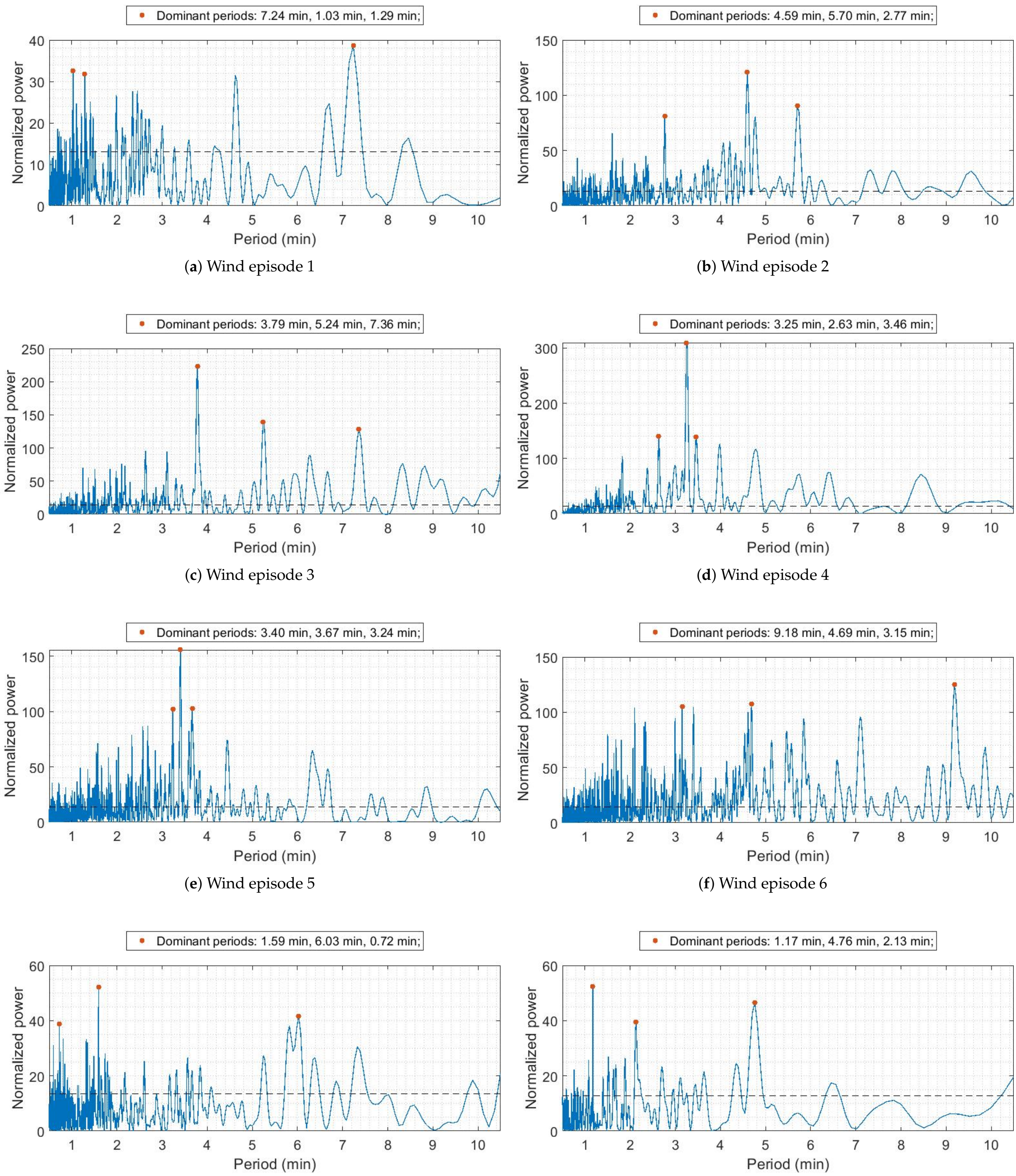

(**a**) Wind episode 1 (**b**) Wind episode 2

(**c**) Wind episode 3 (**d**) Wind episode 4

(**e**) Wind episode 5 (**f**) Wind episode 6

(**g**) Wind episode 7 (**h**) Wind episode 8

Figure 16. Periodograms of vertical wind speed, obtained at 110 m AGL for all eight wind episodes. Horizontal black dashed line represents 0.001 significance level. Dominant periods are given in the legend for each episode.

4. Conclusions

In this study, the properties of a wind flow over a complex terrain in a Bora-affected region in SW Slovenia, the Vipava valley, were investigated using Doppler wind lidar measurements. The measurements of wind velocity were acquired at 21 different height levels in the lower troposphere, from which, heights between 80 and 180 m were studied, covering a thus far uninvestigated vertical range of the atmosphere above the valley floor. Based on eight wind episodes related to Bora that occurred during November and December 2019, the turbulence characteristics and periodicity of the flow over a complex valley environment were assessed.

The turbulence characteristics of the Bora flow were assessed by evaluating turbulence intensity values in the along-wind, lateral and vertical direction and by approximating the along-wind length scales related to all three velocity components. The majority of the analyzed wind episodes exhibited high levels of turbulence intensity, which were found to be considerably greater than the standard values for this type of terrain category. The large values of turbulence intensity may be partly due to the turbulence overestimation by the Doppler wind lidar, but also due to both the lidar's scanning method in the complex environment and atmospheric processes related to the flow passing over a large mountain barrier, which surrounds the valley (such as flow separation, recirculation and reattachment phenomena). The ratios between different intensity components were found to differ from the ones suggested by international standards. Whereas the lateral intensity component was found to be comparable to the along-wind one and was larger than predicted by the standards, the vertical intensity was found to be considerably smaller. Based on eight Bora episodes, we found that, in the Vipava valley case, the relationship between along-wind, lateral and vertical intensity components is best described by the ratio 1:0.9:0.3. Adopting approximations from standards, e.g., for modeling and assessing the effects of wind on structures, may therefore not be the most accurate choice for the case of Bora in the complex terrain.

Turbulence length scales in the along-wind direction, related to the velocity fluctuations in all three directions, were evaluated. It is important to note that the turbulence scales were reported here in an approximate manner, as considerable uncertainties related to the calculation procedure and lidar scanning technique were present in their estimation. The turbulence length scales were found to vary widely between different Bora episodes, with mean values ranging from approximately 40 to 120 m for the L_u^x and L_v^x, and up to 225 m for L_w^x. The vertical profiles of all three along-wind length scales were found to differ from those suggested by international standards ESDU and Eurocode for the terrain category describing the Vipava valley. Whereas L_u^x and L_v^x were found to be moderately comparable with the ESDU standard, L_w^x showed considerable disagreement, reaching considerably larger values than the other two along-wind length scales.

The periodicity of atmospheric flow above the valley was assessed by calculating the periodograms of the vertical wind velocity component, yielding a range of possible periods between 1 and 10 min, which agrees with previous results from the studies of atmospheric flow in the Vipava valley at the heights above 200 m. Further work is required in order to fully characterize the turbulence during Bora episodes in the valley, as well as in other Bora-affected regions in Slovenia, such as: a longer measurement campaign, which would include a larger number of Bora episodes during different seasons; an evaluation of turbulence characteristics with more appropriate tools/techniques; an assessment of the flow characteristics in the near-ground range, below currently assessed heights (i.e., below 80 m); an evaluation of turbulence characteristics with respect to different terrain types and surroundings.

Author Contributions: All of the authors made contributions to this research work and manuscript. In addition to manuscript preparation, M.B. contributed to data analysis, S.S., K.B. and G.M. contributed to research design and L.W. and X.S. contributed to data collection and the review of the manuscript. All authors have read and agreed to the published version of the manuscript.

Funding: This research was supported by Slovenian Research Agency, grants no. P1-0385 and I0-0033, by the National Key Research and Development Program of China, grants no. 2018YFC0213101 and 2016YFC1400905 and by the National Natural Science Foundation of China, grant no. 62105248.

Data Availability Statement: Data presented in this study are available on request from the corresponding author.

Conflicts of Interest: The authors declare no conflict of interest.

Abbreviations

The following abbreviations are used in this manuscript:

ABL	Atmospheric Boundary Layer
AGL	Above the Ground Level
DBS	Doppler Beam Swinging
CWE	Computational Wind Engineering
DWL	Doppler Wind Lidar
EC	Eurocode
LOS	Line-of-Sight
NE	Northeast
SE	Southeast
SNR	Signal-to-Noise Ratio
SW	Southwest
UNG	University of Nova Gorica

Appendix A

Wind directions during eight Bora episodes in the Vipava valley are presented here by wind roses.

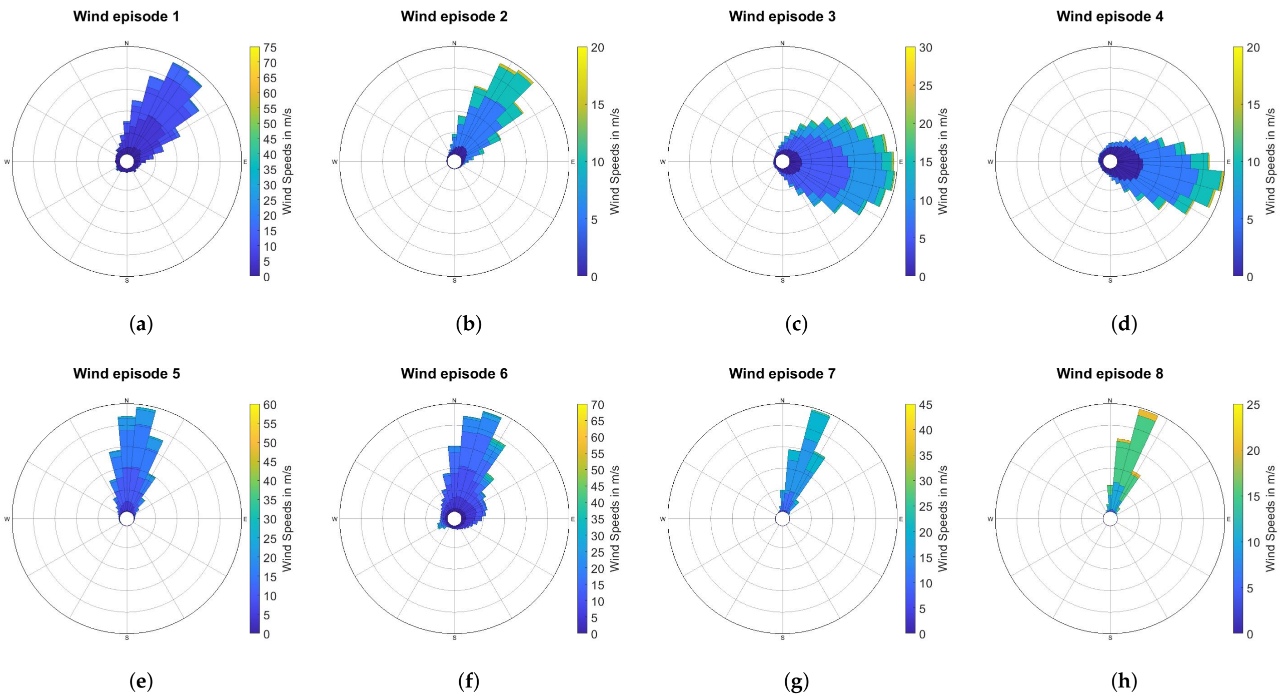

Figure A1. Cumulative wind speed and direction distribution for the heights between 80 and 180 m at measurement site in Ajdovščina during eight Bora episodes in November and December 2019.

Appendix B

Values of turbulence intensity and turbulence integral length scales are reported in Tables A1 and A2, respectively, for selected wind episodes in November-December 2019. Median, arithmetic mean, standard deviation, minimum and maximum values of turbulence quantities are given for four different heights above the ground: 80, 110, 140 and 180 m.

Table A1. Main characteristics of turbulence intensity in the along-wind, lateral and vertical direction: median, mean, standard deviation (σ), minimum and maximum values at four different heights are given for eight wind episodes.

Wind Episode	Turbulence Quantity	Height (m)	Median	Mean	σ	Min	Max
1	I_u (%)	110	60.91	58.62	6.10	47.47	68.38
		140	41.53	42.88	5.30	35.66	53.13
		180	39.29	40.15	6.40	32.06	55.20
	I_v (%)	110	46.22	44.83	5.51	33.71	52.66
		140	34.90	36.05	5.64	31.26	51.76
		180	33.64	35.53	7.56	29.14	55.03
	I_w (%)	110	13.80	13.37	1.49	10.37	15.26
		140	11.79	11.77	1.80	9.64	16.33
		180	11.89	11.47	2.09	8.16	16.21
2	I_u (%)	80	33.30	35.25	5.96	27.21	49.37
		110	32.07	32.82	7.89	24.37	54.69
		140	35.50	37.04	6.71	28.10	51.98
		180	50.40	51.04	6.51	38.30	61.85
	I_v (%)	80	26.67	28.98	5.56	22.25	43.34
		110	28.11	28.47	3.75	23.60	34.91
		140	31.37	32.90	4.04	28.38	41.36
		180	41.97	43.35	6.47	35.84	56.56
	I_w (%)	80	8.30	9.03	1.80	7.14	12.68
		110	7.45	8.39	1.82	6.79	12.28
		140	8.29	9.10	2.01	7.41	14.97
		180	11.52	11.95	2.33	8.69	18.35
3	I_u (%)	80	43.62	45.53	7.52	33.91	63.70
		110	46.35	46.03	7.13	34.29	60.40
		140	47.43	48.33	8.97	32.91	63.03
		180	50.95	51.18	10.19	34.52	68.19
	I_v (%)	80	41.69	41.59	6.83	29.56	63.71
		110	40.70	41.09	6.03	29.88	54.70
		140	41.39	41.98	5.47	31.61	54.57
		180	43.47	45.08	6.60	33.93	62.37
	I_w (%)	80	15.23	15.32	2.52	10.06	19.55
		110	15.75	15.73	2.45	11.34	19.27
		140	17.18	16.45	2.74	11.79	19.93
		180	17.59	17.37	2.71	12.23	21.72
4	I_u (%)	80	47.30	50.99	13.03	38.96	83.27
		110	48.91	52.44	14.21	37.60	86.72
		140	52.40	56.85	15.45	39.45	85.27
		180	54.89	60.51	14.64	45.22	95.95
	I_v (%)	80	43.43	50.03	14.40	35.64	77.66
		110	41.37	47.09	14.60	32.45	76.06
		140	44.89	46.90	12.64	32.21	65.73
		180	49.04	51.08	11.74	35.23	78.93
	I_w (%)	80	15.09	16.23	3.29	11.75	22.53
		110	16.37	17.00	3.18	13.90	24.56
		140	17.44	17.37	3.49	13.91	27.24
		180	16.89	17.50	3.40	12.81	24.21

Table A1. *Cont.*

Wind Episode	Turbulence Quantity	Height (m)	Median	Mean	σ	Min	Max
5	I_u (%)	80	31.12	32.04	5.73	25.92	50.59
		110	30.27	30.89	7.15	21.43	54.50
		140	31.84	32.58	5.99	23.91	51.88
		180	42.01	43.96	9.30	25.32	64.39
	I_v (%)	80	29.62	30.69	6.62	22.17	57.75
		110	29.23	29.63	5.22	20.93	46.62
		140	30.79	30.88	4.49	24.00	40.58
		180	39.70	40.66	7.43	27.09	55.80
	I_w (%)	80	9.63	9.84	1.56	7.35	13.75
		110	9.72	9.89	1.81	6.50	14.47
		140	10.08	10.06	1.76	7.06	14.29
		180	12.18	12.11	2.04	8.28	17.06
6	I_u (%)	80	42.23	47.17	12.67	30.48	79.37
		110	40.23	46.99	15.41	27.17	82.58
		140	59.68	58.98	8.74	35.01	77.08
		180	70.54	69.22	9.25	37.68	85.04
	I_v (%)	80	36.91	42.54	12.79	26.79	76.26
		110	32.24	40.72	14.46	23.91	73.33
		140	46.37	49.65	12.19	29.16	80.72
		180	61.43	60.06	9.78	28.74	77.95
	I_w (%)	80	11.62	14.38	5.39	8.34	28.02
		110	11.03	14.40	6.18	7.73	29.12
		140	14.94	16.56	4.62	9.44	27.21
		180	17.84	18.57	3.37	11.01	28.10
7	I_u (%)	80	20.61	20.42	2.69	15.05	24.57
		110	18.13	17.95	3.01	11.04	22.25
		140	17.61	17.92	3.49	10.86	25.46
		180	29.26	27.22	7.92	16.17	38.34
	I_v (%)	80	20.75	20.60	3.90	12.11	26.54
		110	18.89	17.67	3.25	9.81	21.45
		140	16.94	16.63	3.98	9.17	26.40
		180	18.02	18.80	4.40	13.01	31.04
	I_w (%)	80	6.04	6.14	0.94	3.96	7.53
		110	5.42	5.19	0.99	3.12	6.77
		140	4.83	4.75	0.85	3.08	6.43
		180	5.89	6.01	1.25	4.02	7.64
8	I_u (%)	80	20.09	19.98	2.92	15.82	24.22
		110	17.81	17.48	2.89	13.45	20.86
		140	15.33	15.64	2.32	11.87	18.57
		180	14.72	15.31	2.52	11.84	18.61
	I_v (%)	80	19.47	19.60	4.31	13.61	26.89
		110	17.59	17.02	3.40	12.00	22.38
		140	14.59	16.02	2.87	13.54	20.92
		180	13.40	14.59	2.75	10.99	17.99
	I_w (%)	80	6.13	5.97	0.90	4.12	6.93
		110	5.53	5.22	0.87	3.33	6.12
		140	4.81	4.73	0.63	3.49	5.48
		180	4.37	4.37	0.49	3.52	4.97

Table A2. Main characteristics of turbulence integral length scale in the along-wind direction, related to the velocity fluctuations in all three spatial directions: median, mean, standard deviation (σ), minimum and maximum values at four different heights are given for eight wind episodes.

Label	Turbulence Quantity	Height (m)	Median	Mean	σ	Min	Max
1	L_u^x (m)	110	27.21	33.37	13.81	18.55	54.69
		140	47.95	46.37	18.59	17.89	70.25
		180	42.32	40.68	16.60	16.28	62.94
	L_v^x (m)	110	27.57	29.30	7.13	19.52	42.50
		140	32.76	33.59	7.91	22.54	47.51
		180	43.05	46.37	27.91	16.69	112.87
	L_w^x (m)	110	35.08	40.19	17.17	24.16	85.02
		140	71.65	71.67	13.56	50.34	91.96
		180	88.32	89.58	32.29	39.59	145.31
2	L_u^x (m)	80	33.63	53.26	39.07	17.83	145.47
		110	33.78	59.64	56.99	21.93	201.03
		140	63.22	61.13	36.25	24.31	160.76
		180	39.92	50.15	23.42	23.06	91.33
	L_v^x (m)	80	23.19	29.25	11.53	16.73	48.41
		110	42.63	40.86	12.74	23.49	67.96
		140	45.17	51.48	17.83	31.34	89.88
		180	57.65	64.29	25.25	33.18	107.74
	L_w^x (m)	80	60.27	63.56	26.01	28.87	123.37
		110	65.20	82.37	54.57	34.51	257.51
		140	79.24	97.81	58.87	34.36	234.22
		180	72.65	82.17	51.31	20.73	244.24
3	L_u^x (m)	80	92.54	122.02	83.00	34.24	365.20
		110	89.77	111.57	65.96	33.19	300.91
		140	77.10	99.92	62.55	37.58	322.51
		180	67.76	85.76	59.54	44.69	342.20
	L_v^x (m)	80	80.11	96.23	54.85	35.03	240.56
		110	90.23	100.94	54.83	45.50	250.42
		140	94.20	106.19	50.44	52.12	231.46
		180	96.09	121.70	60.77	41.29	280.28
	L_w^x (m)	80	92.67	135.35	130.61	47.01	648.41
		110	116.97	172.50	169.69	61.40	869.76
		140	150.15	200.15	169.65	81.23	870.30
		180	162.44	220.75	182.35	99.10	901.32
4	L_u^x (m)	80	60.23	60.03	22.88	26.34	113.62
		110	53.81	58.45	19.30	35.46	101.22
		140	61.70	62.62	17.87	37.12	96.94
		180	69.78	76.20	29.86	38.89	143.38
	L_v^x (m)	80	66.99	69.60	32.95	31.81	146.91
		110	63.06	75.29	31.49	44.15	139.99
		140	74.50	92.98	50.93	36.87	208.35
		180	79.85	87.23	49.60	43.28	225.29
	L_w^x (m)	80	77.28	79.40	25.84	44.73	125.29
		110	104.08	100.36	24.89	54.91	140.82
		140	114.88	112.31	34.81	53.46	171.63
		180	123.29	119.93	31.44	61.61	162.18

Table A2. *Cont.*

Label	Turbulence Quantity	Height (m)	Median	Mean	σ	Min	Max
5	L_u^x (m)	80	93.74	98.34	40.78	29.74	187.96
		110	72.70	80.69	52.14	27.25	273.98
		140	66.59	81.37	46.01	27.12	186.17
		180	74.57	86.21	60.68	27.84	324.17
	L_v^x (m)	80	54.78	59.81	22.93	30.10	141.43
		110	75.26	78.22	30.12	32.33	157.00
		140	86.69	97.22	38.55	47.81	195.73
		180	84.20	96.66	54.96	41.04	261.64
	L_w^x (m)	80	110.40	115.65	37.31	59.78	197.77
		110	123.04	130.57	41.89	69.77	289.18
		140	134.42	149.25	52.74	91.53	313.54
		180	125.94	138.69	73.00	34.10	330.13
6	L_u^x (m)	80	58.42	80.40	63.06	18.24	365.50
		110	61.91	78.81	58.92	27.51	343.89
		140	40.97	62.99	58.42	25.29	356.09
		180	49.40	75.36	63.32	29.89	341.25
	L_v^x (m)	80	54.88	72.65	54.31	28.20	286.26
		110	60.81	77.79	55.23	28.19	312.24
		140	62.08	71.76	48.78	27.44	258.06
		180	61.42	73.90	45.18	30.65	246.03
	L_w^x (m)	80	86.36	94.84	40.43	39.01	221.49
		110	122.62	128.38	50.17	49.33	252.67
		140	104.35	114.53	59.70	30.05	301.63
		180	103.96	114.96	70.35	33.48	314.81
7	L_u^x **(m)**	80	62.05	65.59	33.76	27.10	138.49
		110	44.91	62.76	37.85	31.87	158.78
		140	41.29	48.97	17.51	32.56	94.73
		180	40.78	58.52	67.12	26.38	315.58
	L_v^x (m)	80	62.62	67.67	27.80	34.90	148.72
		110	64.32	77.89	31.66	48.59	140.84
		140	77.47	87.24	37.35	41.24	166.82
		180	67.99	86.52	56.10	45.16	279.69
	L_w^x (m)	80	83.74	109.77	84.48	54.05	398.95
		110	83.22	94.14	36.09	54.81	180.29
		140	96.53	98.37	30.50	63.02	187.93
		180	78.98	105.90	112.47	32.42	518.24
8	L_u^x (m)	80	63.91	79.29	57.46	30.28	204.88
		110	50.90	61.55	24.15	36.52	97.82
		140	39.60	64.81	48.03	31.51	154.56
		180	57.76	75.16	54.87	32.49	203.19
	L_v^x (m)	80	50.10	69.17	55.84	39.48	206.17
		110	67.25	71.85	17.94	53.91	108.87
		140	75.67	91.80	32.78	62.54	152.80
		180	100.62	125.20	104.36	55.21	377.60
	L_w^x (m)	80	77.07	83.82	33.23	47.56	133.57
		110	161.57	198.06	126.50	73.27	429.44
		140	179.95	206.12	94.74	95.62	383.66
		180	251.85	225.94	102.50	81.45	344.09

References

1. Köpp, F. Doppler Lidar for Atmospheric Remote Sensing and Aircraft Safety Operations. In *Laser in der Umweltmeßtechnik/Laser in Remote Sensing*; Springer: Berlin/Heidelberg, Germany, 1994; pp. 150–159.
2. Mortensen, N. Wind measurements for wind energy applications—A review. In Proceedings of the 16th British Wind Energy Association Conference', Stirling, Scotland, 15–17 September 1994; pp. 353–360.
3. Zhang, H.; Xu, T.; Zong, Y.; Tang, H.; Liu, X.; Wang, Y. Influence of meteorological conditions on pollutant dispersion in street canyon. *Procedia Eng.* **2015**, *121*, 899–905. [CrossRef]
4. Grubišić, V.; Doyle, J.D.; Kuettner, J.; Mobbs, S.; Smith, R.B.; Whiteman, C.D.; Dirks, R.; Czyzyk, S.; Cohn, S.A.; Vosper, S.; et al. The Terrain-Induced Rotor Experiment: A field campaign overview including observational highlights. *Bull. Am. Meteorol. Soc.* **2008**, *89*, 1513–1534. [CrossRef]
5. Krishnamurthy, R.; Calhoun, R.; Billings, B.; Doyle, J. Wind turbulence estimates in a valley by coherent Doppler lidar. *Meteorol. Appl.* **2011**, *18*, 361–371. [CrossRef]
6. Gan, C.; Salim, S. Numerical analysis of fluid–structure interaction between wind flow and trees. In Proceedings of the World Congress on Engineering, London, UK, 2–4 July 2014; Volume 2, pp. 1218–1223.
7. Laidlaw, D.J.; Osborn, J.; Morris, T.J.; Basden, A.G.; Gendron, E.; Rousset, G.; Townson, M.J.; Wilson, R.W. Automated wind velocity profiling from adaptive optics telemetry. *Mon. Not. R. Astron. Soc.* **2020**, *491*, 1287–1294. [CrossRef]
8. Wang, Z.; Zhang, L.; Kong, L.; Bao, H.; Guo, Y.; Rao, X.; Zhong, L.; Zhu, L.; Rao, C. A modified S-Dimm+: Applying additional height grids for characterizing daytime seeing profiles. *Mon. Not. R. Astron. Soc.* **2018**, *478*, 1459–1467. [CrossRef]
9. Shikhovtsev, A.Y.; Kiselev, A.; Kovadlo, P.; Kolobov, D.Y.; Lukin, V.; Tomin, V. Method for estimating the altitudes of atmospheric layers with strong turbulence. *Atmos. Ocean. Opt.* **2020**, *33*, 295–301. [CrossRef]
10. Liu, Z.; Barlow, J.F.; Chan, P.W.; Fung, J.C.H.; Li, Y.; Ren, C.; Mak, H.W.L.; Ng, E. A Review of Progress and Applications of Pulsed Doppler Wind LiDARs. *Remote Sens.* **2019**, *11*, 2522. [CrossRef]
11. Jaynes, D.W.; McGowan, J.G.; Rogers, A.L.; Manwell, J.F. Validation of Doppler lidar for wind resource assessment applications. In Proceedings of the American Wind Energy Association WindPower 2007 Conference and Exhibition, Los Angeles, CA, USA, 3–7 June 2007.
12. Krishnamurthy, R.; Boquet, M.; Osler, E. Current Applications of Scanning Coherent Doppler Lidar in Wind Energy Industry. In *EPJ Web of Conferences*; EDP Sciences: Les Ulis, France, 2016; Volume 119, p. 10003.
13. Gohm, A.; Mayr, G.J.; Fix, A.; Giez, A. On the onset of bora and the formation of rotors and jumps near a mountain gap. *Q. J. R. Meteorol. Soc.* **2008**, *134*, 21–46. [CrossRef]
14. Mole, M.; Wang, L.; Stanič, S.; Bergant, K.; Eichinger, W.E.; Ocaña, F.; Strajnar, B.; Škraba, P.; Vučković, M.; Willis, W.B. Lidar measurements of Bora wind effects on aerosol loading. *J. Quant. Spectrosc. Radiat. Transf.* **2017**, *188*, 39–45. [CrossRef]
15. Wang, L.; Stanič, S.; Bergant, K.; Eichinger, W.; Močnik, G.; Drinovec, L.; Vaupotič, J.; Miler, M.; Gosar, M.; Gregorič, A. Retrieval of Vertical Mass Concentration Distributions—Vipava Valley Case Study. *Remote Sens.* **2019**, *11*, 106. [CrossRef]
16. Wang, L.; Stanič, S.; Eichinger, W.; Močnik, G.; Drinovec, L.; Gregorič, A. Investigation of Aerosol Properties and Structures in Two Representative Meteorological Situations over the Vipava Valley Using Polarization Raman LiDAR. *Atmosphere* **2019**, *10*, 128. [CrossRef]
17. Wang, L.; Bervida, M.; Stanič, S.; Bergant, K.; Eichinger, W.; Strajnar, B. Lidar Observations of Mountain Waves During Bora Episodes. In *EPJ Web of Conferences*; EDP Sciences: Les Ulis, France, 2020; Volume 237.
18. Bervida, M.; Stanič, S.; Bergant, K.; Strajnar, B. Near-Ground Profile of Bora Wind Speed at Razdrto, Slovenia. *Atmosphere* **2019**, *10*, 601. [CrossRef]
19. QINGDAO Leice Transient Technology Co., Ltd. Available online: http://leice-lidar.com/en/product-3-35.html (accessed on 24 June 2020).
20. Schrader, P. Computing the statistical stability of integral length scale measurements by autoregressive simulation. In *Computational Wind Engineering 1*; Elsevier: Amsterdam, The Netherlands, 1993; pp. 487–496.
21. VanderPlas, J.T. Understanding the Lomb–Scargle Periodogram. *Astrophys. J. Suppl. Ser.* **2018**, *236*, 16. [CrossRef]
22. Mole, M. Study of the Properties of Air Flow over Orographic Barrier. Ph.D. Thesis, Nova Gorica University, Nova Gorica, Slovenija, 2017.
23. Slovenian Environment Agency: Monthly Bulletin. Available online: http://www.arso.gov.si/o%20agenciji/knji%C5%BEnica/mese%C4%8Dni%20bilten/bilten2019.htm (accessed on 10 September 2020).
24. DARS. Arhiv Meritev. Available online: https://www.promet.si/portal/sl/merilna-mesta-sistema-burja.aspx (accessed on 10 September 2020).
25. Lepri, P.; Kozmar, H.; Večenaj, Ž.; Grisogono, B. A summertime near-ground velocity profile of the Bora wind. *Wind. Struct.* **2014**, *19*, 505–522. [CrossRef]
26. Fuad, M.A.Z. *Coral Reef Rugosity and Coral Biodiversity*; Bunaken National Park: North Sulawesi, Indonesia, 2010.
27. Suomi, I.; Gryning, S.E.; O'Connor, E.J.; Vihma, T. Methodology for obtaining wind gusts using Doppler lidar. *Q. J. R. Meteorol. Soc.* **2017**, *143*, 2061–2072. [CrossRef]
28. Report: Calibration Test of WindMast WP350. Available online: https://mgwtradenservice.com.au/wp-content/uploads/2020/06/RSV19018_A1_Calibration-of-WindMast_WP350_final-Windguard.pdf (accessed on 12 August 2020).

29. Wang, H.; Barthelmie, R.J.; Clifton, A.; Pryor, S.C. Wind Measurements from Arc Scans with Doppler Wind Lidar. *J. Atmos. Ocean. Technol.* **2015**, *32*, 2024–2040. [CrossRef]
30. Pauscher, L.; Vasiljevic, N.; Callies, D.; Lea, G.; Mann, J.; Klaas, T.; Hieronimus, J.; Gottschall, J.; Schwesig, A.; Kühn, M.; et al. An inter-comparison study of multi-and DBS lidar measurements in complex terrain. *Remote Sens.* **2016**, *8*, 782. [CrossRef]
31. EN 1991–1–4:2005 (sl) Evrokod 1: Vplivi na konstrukcije—1-4.del: Splošni vplivi—Vplivi vetra. Available online: https://www.gzs.si/zbornica_gradbenistva_in_industrije_gradbenega_materiala/vsebina/Gradbeni-standardi/Evrokodi-evropski-standardi (accessed on 8 August 2019).
32. Wiernga, J. Representative roughness parameters for homogeneous terrain. *Bound.-Layer Meteorol.* **1993**, *63*, 323–363. [CrossRef]
33. Bervida, M.; Patruno, L.; Stanič, S.; de Miranda, S. Synthetic generation of the atmospheric boundary layer for wind loading assessment using spectral methods. *J. Wind. Eng. Ind. Aerodyn.* **2020**, *196*, 104040. [CrossRef]
34. Dyrbye, C.; Hansen, S.O. *Wind Loads on Structures*; John Wiley & Sons: Hoboken, NJ, USA, 1997.
35. Holmes, J.D. *Wind Loading of Structures*; Spon Press: London, UK, 2001.
36. Lepri, P.; Večenaj, Ž.; Kozmar, H.; Grisogono, B. Near-ground turbulence of the Bora wind in summertime. *J. Wind. Eng. Ind. Aerodyn.* **2015**, *147*, 345–357. [CrossRef]
37. ESDU. *Characteristics of Atmospheric Turbulence Near the Ground*; Engineering Sciences Data Unit, IHS Group: London, UK, 2001.
38. Flay, R.; Stevenson, D. Integral length scales in strong winds below 20 m. *J. Wind. Eng. Ind. Aerodyn.* **1988**, *28*, 21–30. [CrossRef]
39. Shiau, B.S. Velocity spectra and turbulence statistics at the northeastern coast of Taiwan under high-wind conditions. *J. Wind. Eng. Ind. Aerodyn.* **2000**, *88*, 139–151. [CrossRef]
40. Petkovšek, Z. Periodicity of Bora Gusts. *Razprave* **1976**, *20*, 67–75.
41. Belušić, D.; Pasarić, M.; Orlić, M. Quasi-periodic Bora gusts related to the structure of the troposphere. *Q. J. R. Meteorol. Soc.* **2004**, *130*, 1103–1121. [CrossRef]
42. Belušić, D.; Žagar, M.; Grisogono, B. Numerical simulation of pulsations in the bora wind. *Q. J. R. Meteorol. Soc.* **2007**, *133*, 1371–1388. [CrossRef]